Journal of
Composites Science

MDPI

Article

Easily Processable Thermoplastic Microcomposites with Enhanced UV Shielding Performance Based on Anionic Polyamide 6 and Sulfonated Lignin

Marco Papparotto [1], Roberto Miani [2], Pavel Solovyev [3], Edoardo Zonta [1], Alessandro Sorze [1], Andrea Dorigato [1], Claudio Gioia [2,*] and Giulia Fredi [1,*]

[1] Department of Industrial Engineering and INSTM Research Unit, University of Trento, Via Sommarive 9, 38123 Trento, Italy; marco.papparotto@unitn.it (M.P.); edoardo.zonta@unitn.it (E.Z.); alessandro.sorze@unitn.it (A.S.); andrea.dorigato@unitn.it (A.D.)
[2] Department of Physics, University of Trento, Via Sommarive 14, 38123 Trento, Italy; roberto.miani@unitn.it
[3] Edmund Mach Foundation, Via Edmund Mach 1, 38098 San Michele all'Adige, Italy; pavel.solovyev@fmach.it
* Correspondence: claudio.gioia@unitn.it (C.G.); giulia.fredi@unitn.it (G.F.); Tel.: +39-0461282770 (G.F.)

Abstract

Anionic polyamide 6 (aPA6) thermoplastic composites are known for their excellent mechanical and functional properties, including high strength, toughness, good processability, and gas-barrier capabilities. However, when exposed to the environment, they seem to lack proper mechanisms to resist degradation from radiation and atmospheric agents. For this reason, in this paper, the incorporation of a microscopic bio-based sulfonated lignin filler was investigated, aiming to improve UV shielding properties, which are expected to prolong the life cycle of the material and to decrease microplastic formation with extensive environmental benefits. In this work, anionic ring-opening polymerization (AROP) of ε-caprolactam (CL) was employed for the first time to produce aPA6/lignin microcomposites containing up to 5 wt% lignin in a simple in situ one-pot process. A marked increase in attenuation coefficient was observed in the UV range, up to 894% at 346 nm. Nuclear magnetic resonance (NMR) and microscopic characterization excluded chemical bonding between biofiller and matrix, resulting in a moderate decrease in mechanical performance (−21.4% in yield strength and −16.3% in stress at break). However, the absence of lignin–PA6 hybrids may be beneficial to the recyclability of the material. Overall, this study proved the benefits of introducing a widely available and environmentally friendly filler into recyclable high-performance composite materials, imparting further functional properties and anticipating novel applications.

Keywords: anionic polyamide 6; lignin; UV-protection; thermoplastic resin transfer molding; microcomposites; NMR

Check for updates

Academic Editor: Yang Li

Received: 25 September 2026
Revised: 24 October 2026
Accepted: 26 October 2026
Published: 29 October 2026

Copyright: © 2026 by the authors. Licensee MDPI, Basel, Switzerland. This article is an open access article distributed under the terms and conditions of the Creative Commons Attribution (CC BY) license.

1. Introduction

In the context of a plastic and composite industry that is facing new environmental challenges [1,2], sustainability is becoming a central design aspect. For polymer composites, solutions such as the addition of renewable bio-based or natural fillers [3], the replacement of traditional thermosetting matrices with recyclable thermoplastic alternatives [4,5], and the design for improved durability and prolonged life-cycle of products [6–10] are acquiring great relevance.

Thermoplastic composites are gaining attention due to their high toughness, inherent weldability, and recyclability. However, the high processing temperatures required for engineering thermoplastics like polyamide 6 and polyamide 66 often prevent the incorporation of many bio-based fillers as reinforcement in this type of material because natural fibers and fillers tend to have lower degradation temperatures with respect to other traditional reinforcements such as carbon, glass, and basalt fibers [11]. Therefore, reactive processing has emerged as a promising technology to produce thermoplastic composites with such heat-sensitive fillers [11]. Not only are the temperatures involved generally lower than the melting temperature (T_m) of the polymeric matrix, but this type of processing also permits proper incorporation of fillers because of the low viscosities involved [4], and it has shown compatibility with "grafting from" reactions [12]. Reactive processing consists of the use of monomers or oligomers, and possibly catalysts, to promote the polymerization of the matrix in situ, generally inside a mold, along with the selected filler [4]. Polyamide 6 (PA6), in particular, has a melting temperature of approximately 214–220 °C [13], rendering typical processing routes for PA6 composites incompatible with many bio-based fillers. However, it is possible to employ alternative reactive processing routes such as thermoplastic-resin transfer molding (T-RTM) for this purpose. T-RTM of PA6 relies on the anionic ring-opening polymerization (AROP) of ε-caprolactam (CL), which can be transferred in the molten state into a heated mold (T~150 °C) along with appropriate catalysts and fillers to polymerize in situ and produce high-performance composites, possibly containing bio-based fillers, with excellent fiber-matrix adhesion [5]. Anionically polymerized PA6 (aPA6) is thus considered a promising thermoplastic matrix due to its high performance and low processing temperatures [5]. However, aPA6 has some important limitations, notably the moisture sensitivity of the material and of the polymerization reaction, and low ultraviolet radiation (UV) stability [12]. Photodegradation over time can have major impacts on the mechanical properties of the material, but it is also linked to microplastic formation [14], which is a further environmental issue [15]. Several approaches have been proposed to improve the UV stability of PA6, such as grafting PA6 with methyl methacrylate [16], employing SiO_2-TiO_2 nanoparticles [17] or tannic acid- and taurine-based [18] coatings, and employing engineered sizing agents on carbon fibers [19]. However, many of these additives come from non-renewable resources or can negatively affect the recyclability and the environmental impact of the material, particularly at the end of life.

To address these environmental drawbacks, lignin has emerged as a promising sustainable alternative. It is an abundant, biodegradable, and renewable aromatic biopolymer that constitutes one of the main components of plant cell walls and is produced industrially on a large scale, especially by the paper industry [20]. Among the technical lignins produced as by-products of the pulp and paper industry, sodium lignosulfonate from sulfite pulping is a widely available, low-cost feedstock [21]. Characterized by a three-dimensional branched phenol-rich structure, lignin has recently emerged as a promising sustainable biofiller for polymeric materials, imparting interesting functional properties such as flame retardancy [22], UV resistance [23], and antioxidant activity, in particular against UV photooxidation, because of its phenol content [20]. Lignin has been used as a filler in many polymeric matrices, including thermoplastic polymers such as polyethylene (PE) [24], polypropylene (PP) [25], polystyrene (PS) [26], and biopolymers such as polylactic acid (PLA) [27] and polyhydroxyalkanoates [28]. However, it often exhibits poor miscibility due to its tendency to self-aggregate via intermolecular association in the form of strong hydrogen bonds, Van der Waals forces, and π–π stacking, therefore often requiring compatibilization in composite materials applications [29].

Concerning polyamide 6, to the best of our knowledge, few examples in the literature report lignin as a filler [23,30] able to create strong hydrogen bonds between hydroxyl

groups of the lignin and amide moieties, and only recently sodium lignosulfonate was successfully introduced up to 20 wt% by traditional blending to achieve microcomposites presenting enhanced thermomechanical and flame-resistant performances. Indeed, sodium lignosulfonate, presenting polar functionalities, seems a good candidate for improving functional properties of polar polymers, such as PA6, without the use of compatibilizers or chemical modifications. However, to the best of our knowledge, there are no published studies on aPA6/lignosulfonate microcomposites, and the impact of such a biofiller on processing, properties, and compatibility, as well as its influence on the AROP reaction (sensitive to moisture and impurities), has not yet been reported in the literature. Therefore, the present work focuses on the production and characterization of aPA6 microcomposites containing sulfonated lignin in varying concentrations without further compatibilization via T-RTM with a simple in situ one-pot process. This study aims to evaluate the effect of lignin on the processability and on the thermal, mechanical, and functional properties of aPA6. Particular focus is devoted to the UV shielding properties and to the chemical interactions at the interface between aPA6 and lignin.

2. Materials and Methods

2.1. Materials

For the polymerization of polyamide 6, three reagents were used: (i) ε-caprolactam (CL) with commercial name AP-Nylon®; (ii) Bruggolen C10® (sodium caprolactamate in CL); and (iii) Bruggolen C20P® (blocked diisocyanate in CL), all kindly provided by Brüggemann GmbH (Heilbronn, Germany). The filler used was sulfonated lignin powder (L0082) with a density of 1.23 g/cm^3, purchased from Tokyo Chemical Industry Co., Ltd. (Tokyo, Japan). Before storage, lignin was pre-dried at 130 °C for 5 h to remove moisture and other volatile substances. Lignin was then stored in a ventilated oven at 50 °C to maintain low humidity, and PA6 reagents were stored in desiccators under dry conditions.

2.2. Sample Preparation

For the preparation of neat and reinforced samples, a laboratory-scale thermoplastic-resin transfer molding setup was employed, as described in previous work [31]. The polymerization reaction consisted of an anionic ring-opening polymerization of CL. The setup was constituted by a reactive chamber and an aluminum mold, connected through polytetrafluoroethylene (PTFE) tubes. A three-neck round-bottom flask acted as the reactive chamber, which was heated to 110 °C. Inside the chamber, reagents were melted, mixed with the biofiller (when present), and magnetically stirred. The flask was kept under constant nitrogen flux throughout the duration of the process to keep the reagents in anhydrous conditions. The mold contained a cavity of approximately 150 × 150 × 2 mm^3 and was kept at a polymerization temperature of 160 °C.

For sample preparation, the monomer (CL) was added first, along with the initiator (C10). The reagents were allowed to melt and mix for approximately 45–50 min, while residual water was removed due to the temperature and the nitrogen flux. Then, the lignin powder was added directly to the liquid reagents and stirred for approximately 5–10 min to obtain a homogeneous mixture. Finally, the activator (C20P) was added to the flask and mixed for approximately 60 s. Concentrations used were 4.40 phr (parts per hundred resin, i.e., 4.40 g of reagent for 100 g of CL) of C10 and 3.00 phr of C20P, while the lignin was added in 0, 1, 2, and 5 wt% concentrations. The incorporation of higher filler fractions was not possible due to the high amount of moisture apported by the lignin, which would inhibit the polymerization reaction, and because higher filler concentrations could not be readily dispersed in the reactive mixture. The resulting liquid was transferred into the aluminum mold immersing the PTFE tube inside the reactive mixture and applying

a pressure of approximately 1.2 bar with the nitrogen flux in the reactive chamber. The reactive mixture was kept in the mold at a temperature of 160 °C for approximately 90 min to allow for the complete in situ polymerization inside the cavity. The remaining partially reacted liquid was collected in a sprue over the mold. The mold was then opened and the sample was extracted.

Some portions of the samples were ground via cryomilling with an IKA® M 20 universal milling machine by IKA-Werke GmbH & Co. KG (Staufen, Germany) cooled with liquid nitrogen, and approximately 7 g of the obtained powder was pressure molded on a hot press with 7 bar at 240 °C for 10 min to obtain thin films approximately 110 ± 24 µm thick. Two-centimeter-side square specimens for UV–visible spectroscopy were obtained from the thin films via cutting.

Samples were labeled as follows: PA6-N for neat PA6 samples, PA6-XL with X representing the mass percentage of the lignin with respect to the other reagents. For example, PA6-5L indicates a microcomposite sample containing 5 wt% of lignin.

2.3. Characterization Techniques

Scanning electron micrographs (SEM) were obtained on cryofractured samples obtained from representative portions of the samples with a Zeiss SUPRA 40 FE-SEM by Carl Zeiss SMT GmbH (Oberkochen, Germany) after Pt-Pd sputtering.

The samples were extracted in boiling water for 28 h, and the resulting soluble fractions were filtered, washed, and freeze-dried to retrieve and analyze post-reaction lignosulfonate by ^{1}H- ^{13}C- nuclear magnetic resonance (NMR), heteronuclear single quantum coherence (HSQC), and diffusion-ordered spectroscopy (DOSY). ^{1}H- and ^{13}C-NMR were recorded on a Bruker 400 Avance III HD by Bruker Corporation (Billerica, MA, USA) equipped with a BBI-z grad probe head 5 mm (^{1}H: 400 MHz, ^{13}C: 100.5 MHz). The chemical shifts (δ) for ^{1}H and ^{13}C are given in ppm relative to the residual signals of the solvents. For heteronuclear single quantum coherence spectroscopy and diffusion-ordered spectroscopy NMR, the samples were recorded either in D_2O or deuterated DMSO (Deutero GmbH, Kastellaun, Germany, 99.8% isotopic purity containing 0.03% tetramethylsilane (TMS) by volume). The two-dimensional HSQC spectra were recorded at 300 K on a Bruker 600 Avance Neo NMR spectrometer by Bruker Corporation equipped with a broadband 5 mm Z-gradient probe. The acquisition and processing were carried out using TopSpin 4.1.3 software in the automation mode with Icon NMR 5.2.3 using the following experimental parameters: Acquisition time (AQ) was 0.106 s. Delay between the scans (D1) was 2.0 s. The size of the spectral window or sweep width (SW) was 16.02 ppm in F2 and 165 ppm in F1 frequency S4 axis; time domain (TD) was 2048 in F2 and 512 in F1. Number of dummy scans (DS) was 16, and number of scans (NS) was 64. The spectra processing was carried out in the TopSpin software with the size of the real spectrum (SI) set to double value of TD, i.e., 4096 data points for F2 and 1024 data points for F1, using the proc_2dinv automation program. The pseudo-2D DOSY spectra were recorded on Bruker 600 Avance Neo NMR spectrometer equipped with a broadband 5 mm Z-gradient probe with the following parameters: The ledbpgp2sdync pulse program was used. Acquisition was run in automation mode using the au_dosy_dc automation program; acquisition time (AQ) was 1.31 s. Delay between scans (D1) was 3 s; the size of the spectral window or sweep width (SW) was 20.83 ppm in F2 and 10 ppm in F1 frequency axis. Time domain (TD) was 32,768 (32K) data points for F2 and 8 data points for F1. Number of dummy scans was 4, and number of scans (NS) was 16. The spectra processing was carried out in the TopSpin software using the proc_dosy_dc automation program supported by the Bruker Dynamics Center 2.6.1 (2020 Feb/10) software.

Differential scanning calorimetry (DSC) was obtained on representative portions of the samples with a Mettler DSC 30 by Mettler Toledo Inc. (Columbus, OH, USA). Measurements were recorded under nitrogen flow (100 mL/min) with a heating/cooling/heating ramp between 0 °C and 250 °C, at a constant heating/cooling rate of 10 °C/min. Crystallinity of the PA6 matrix was calculated according to Equation (1).

$$\chi\ (\%) = ((\Delta H_m)/(\Delta H_0\ \omega_{PA6})) \cdot 100, \quad (1)$$

where χ is the crystallinity of the PA6; ΔH_m is the melting enthalpy of PA6; ΔH_0 is the theoretical melting enthalpy of fully crystalline PA6, assumed to be 190 J/g [13]; and ω_{PA6} is the nominal mass fraction of the PA6. The melting temperature of PA6 (T_m), taken as the maximum of the peak of the heating scan, and its crystallization temperature (T_c), taken as the maximum of the peak of the cooling scan, were also recorded.

Thermogravimetric analysis (TGA) measurements were obtained on representative portions of the samples with a TG50 MT5 by Mettler Toledo Inc. (Columbus, OH, USA) at 10 °C/min, from 30 to 700 °C under nitrogen flow of 10 mL/min with blank subtraction. The conversion degree (CD) was calculated from the residual mass at 250 °C (Res_{250}) as a first approximation, as reported in [31], according to Equation (2).

$$CD\ (\%) = (((Res_{250}/100) - \omega_{lignin})/\omega_{PA6}) \cdot 100, \quad (2)$$

where ω_{lignin} is the mass fraction of the lignin.

Quasi-static tensile tests on neat and composite samples were performed according to ISO 527-1 [32] with an Instron® 5969 universal testing machine (Norwood, MA, USA), equipped with a 10 kN load cell and applying a sampling rate of 50 Hz. Elastic modulus was measured with the aid of an Instron® 2620-601 extensometer (Norwood, MA, USA) at 0.25 mm/min crosshead speed from 0.05% to 0.25% deformation. The test continued to failure with a 1 mm/min crosshead speed. 1BA tensile specimen geometry (according to ISO 527-2 [33]) was obtained from the molded plates by laser cutting. Eight specimens were tested for each composition.

UV–visible transmittance of films was determined with a Shimadzu UV-2600i spectrophotometer by Shimadzu Italia S.r.l. (Milano, Itay). A wavelength range of 250–850 nm was used, using a step scanning speed of 400 nm/min. Measurements were performed in air. The attenuation coefficient α was calculated using the Beer–Lambert law according to Equation (3).

$$\alpha\ (1/\text{mm}) = (2.303/t) \cdot \text{Log}_{10}(T/100), \quad (3)$$

where T is the transmittance in percentage and t is the thickness of the specimen in mm. This should be considered an approximate value since some effects, such as light scattering and uneven distribution of the filler, could influence the linearity of the Beer–Lambert law.

2.4. Statistical Treatment of Data

Data were reported as mean ± standard deviation, when applicable. Statistical analysis of data was carried out through the Kruskal–Wallis test with a significance level of 0.05 and Dunn's post hoc test.

3. Results and Discussion

3.1. Scanning Electron Microscopy (SEM)

Selected scanning electron micrographs of the neat lignin and of the prepared samples are reported in Figure 1a–f.

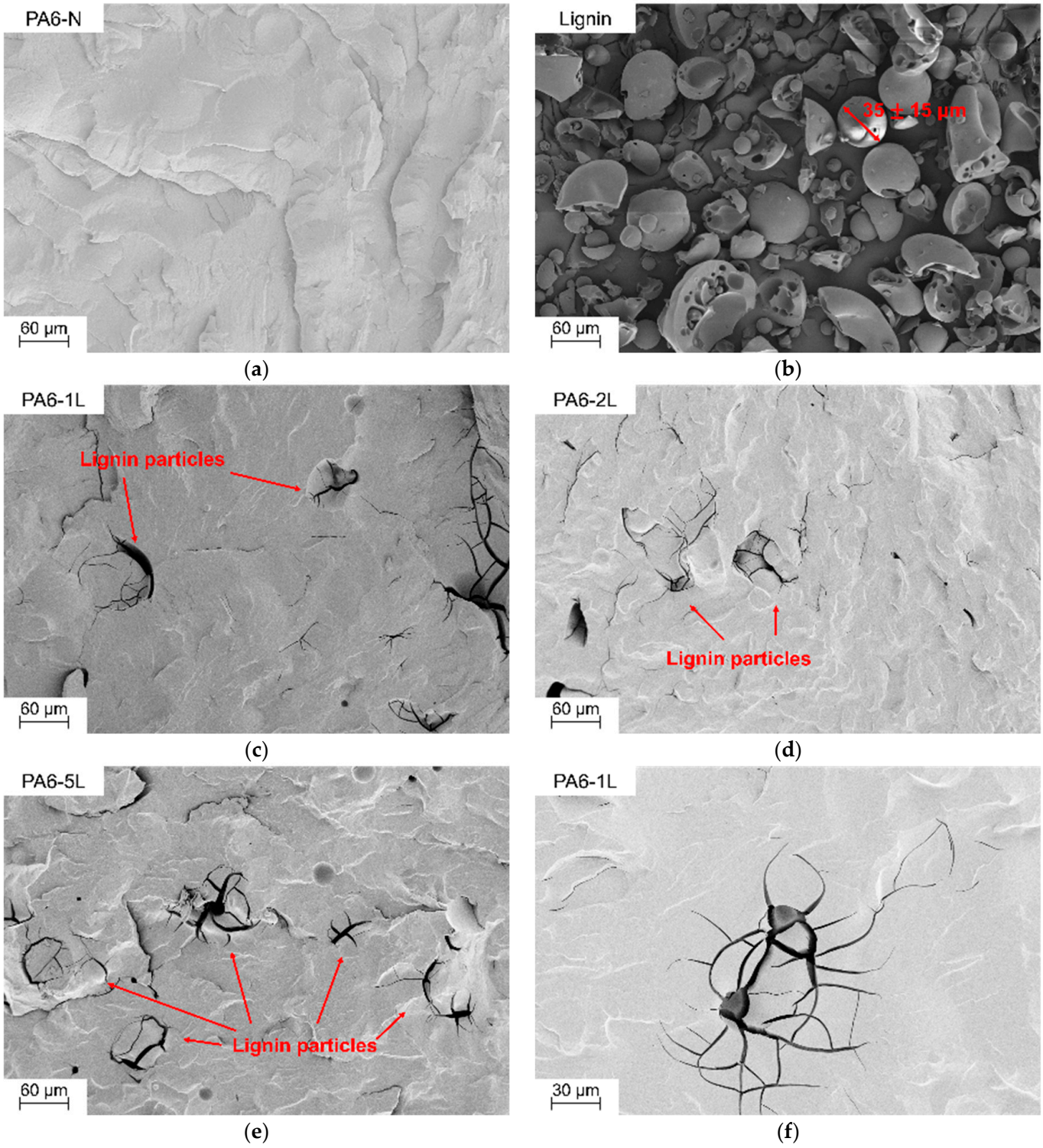


Figure 1. Scanning electron micrographs of (**a**) PA6-N; (**b**) lignin (as-received); (**c**,**f**) PA6-1L; (**d**) PA6-2L; (**e**) PA6-5L samples. All micrographs are taken at 500× magnification, except for (**f**), which is at 1000× magnification.

In Figure 1a, it is possible to observe the microstructure of neat anionic PA6, which appears rather smooth and homogeneous. The shape and dimensions of as-received lignin particles are visible in Figure 1b; the mean diameter of the particles is approximately 64 ± 38 µm. They also show a partially cracked morphology and the presence of porosity. Structures of comparable dimensions and features (with diameter of approximately 70 ± 31 µm) are observed within all samples containing lignin (Figure 1c–f); they appear

approximately circular and severely cracked, sometimes containing porosity, and are likely associated with the lignin biofiller. The interface between particle and matrix cannot be clearly detected, and no obvious gaps can be observed. The particles appear well dispersed, and no significant porosity is observed in any sample outside the particles.

Microscopic characterization via SEM seems to indicate adequate dispersion of the biofiller with the employed method, even though the low lignin concentrations that are compatible with the complex and moisture-sensitive AROP of CL make it difficult to conclusively evaluate the dispersion of the filler, especially in 1 and 2 wt% samples. The processability seems unaffected by the addition of lignin, as highlighted by the substantially similar surface morphology of the matrix in composites and that of the neat sample. The absence of gaps between particles and matrix in most micrographs suggests that the adhesion could be very strong; this is also corroborated by the absence of particle detachment. However, further interfacial strength tests should be performed to confirm good adhesion. The observed structure could be obtained from the partial melting of lignin particles in high temperature caprolactam monomer during processing and subsequent partial interdiffusion of lignin and PA6 at the interface. An in-depth analysis of chemical interactions between aPA6 and lignin is provided in Section 3.2. Only intraparticle cracking is observed, particularly around lignin-apported porosities, which seem to remain unaffected in the final material. These porosities are not observed in [22], possibly because of the different pressures employed in the two works, 4.9 MPa in the processing utilized by Sorze et al., and approximately 0.1 MPa in this work. Ultimately, the affinity between lignin biofiller and aPA6 matrix seems very good, without requiring any compatibilization. The lignin particles themselves, however, seem to impart a substructure characterized by intraparticle cracks and porosities.

3.2. Nuclear Magnetic Resonance (NMR) Spectroscopy

The starting lignin structure was evaluated by HSQC analysis (Figure 2), highlighting the most relevant regions of the bidimensional spectrum, including the aromatic region (Figure 2A) and the oxidized aliphatic region (Figure 2B) [34–40]. The aromatic region confirms the presence of sulfonated units, showing signals deriving from the Sulfo-G units at 7.07/115.3, 6.95–6.57/117.4, and 6.88–6.59/124.6 ppm. Additionally, the signals at 7.19/112.9 ppm and 7.53/117.1 ppm, along with the condensed acid moieties at 7.48/125.3 ppm, testify that the starting lignin was subjected to extensive oxidation processes, leaving carbonyl and carboxylic functional groups. Furthermore, at 7.23/131.8 ppm, stilbene units may be detected. The oxidized aliphatic region (Figure 2B) confirms that the main typical connecting units have been cleaved, possibly leaving only traces of βO4 units at 3.65/64.9 ppm and ββ units at 4.17/171.6 and 2.80/57.4 ppm. Finally, no carbohydrate residues can be detected in the region 5.00–4.50/95.0–110.0 ppm (see Figure S1 in the Supplementary Materials), further confirming the harsh oxidizing conditions applied to this lignin batch. Indeed, the presence of oxidized units as well as sulfonate moieties makes this lignosulfonate feedstock potentially suitable for a proper interaction with the polar amide units in aPA6. The diffusion-ordered spectroscopy experiment (DOSY, Figure S3) shows two populations with distinct diffusion coefficients, which suggests the presence of two different molecular weight groups. Most likely, the starting lignin presents some low-molecular-weight oligomers.

All the prepared PA6-based composites, along with the reference sample PA6-N, were studied by ^{1}H-NMR and ^{13}C-NMR (Figures S4–S11). In all cases, the observed spectra show signals typical of polyamide 6 samples. Lignin contribution seems to be negligible in the structural analysis.

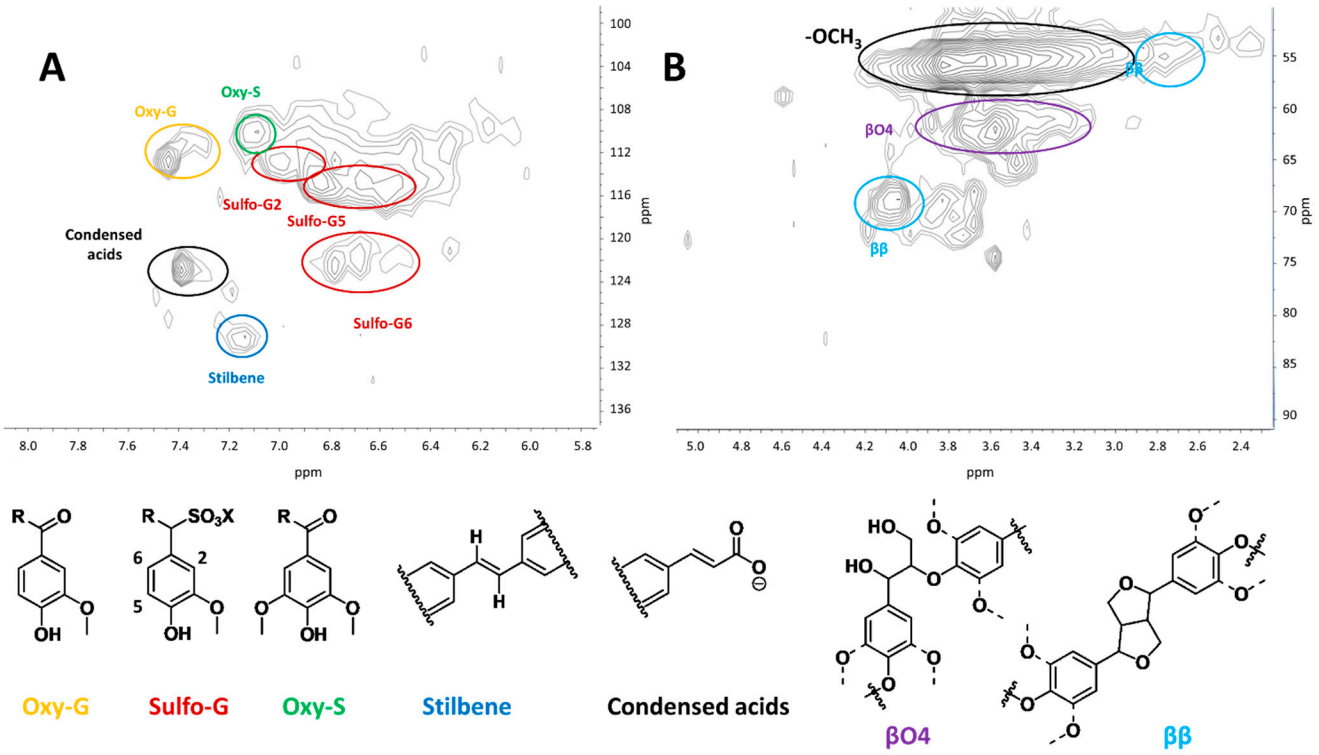


Figure 2. The HSQC analysis of the lignin feedstock: (**A**) aromatic region; (**B**) oxidized aliphatic region.

Hot water extraction was used to retrieve a substantial amount of the lignosulfonate from the composites, allowing for better structural characterization, aiming at understanding possible chemical modification of the lignosulfonate architecture. The yields of the extraction were 0.7%, 1.9%, 3.0%, and 6.4% for PA6-N, PA6-1L, PA6-2L, and PA6-5L, respectively. By assuming lignin as an inert filler ineffective on the polymerization rate, its recovery may be considered substantially complete. The corresponding ^{1}H-NMR analysis (Figures S12, S15, S18, and S21) shows signals deriving from both lignin and PA6 oligomers/monomers. ^{13}C-NMR (Figures S13, S16, S19, and S22) further confirms the presence of a heterogeneous mixture of compounds presenting multiple signals in the 165–180 ppm region. These carbonyl functionalities most likely belong to monomers and oligomers deriving from the low-molecular-weight fraction of PA6, presenting acid and amide functionalities. The presence of multiple species in the reference extracted sample, PA6-N, is further confirmed by the DOSY experiment (Figure S14), presenting species with similar chemical shifts but with different diffusivities.

In Figures 3 and S24, a DOSY experiment was performed on PA6-5L to understand whether the PA6 signals detected in the ^{1}HNMR spectrum belong to units grafted onto lignin architectures or are detached in the mixture of monomeric residues. Indeed, all the sharp signals related to PA6 oligomers (blue) present a diffusion rate ranging between 2.88×10^{-10} and 6.36×10^{-10} m^2s^{-1}, while the broad lignin signals in the aromatic region (7.5–6.5 ppm), the oxidized aliphatic region (4.5–3 ppm) and terminal aliphatic region (0.75 ppm), all present a diffusion rate ranging between 2.40×10^{-10} and 1.03×10^{-10} m^2s^{-1}. Such differences in diffusivity suggest that no grafting of PA6 occurred during polymer synthesis. Figures S17 and S20 report the DOSY experiment also for PA6-1L and PA6-2L. Also in these cases, no obvious proof of PA6–lignin linkage is detected.

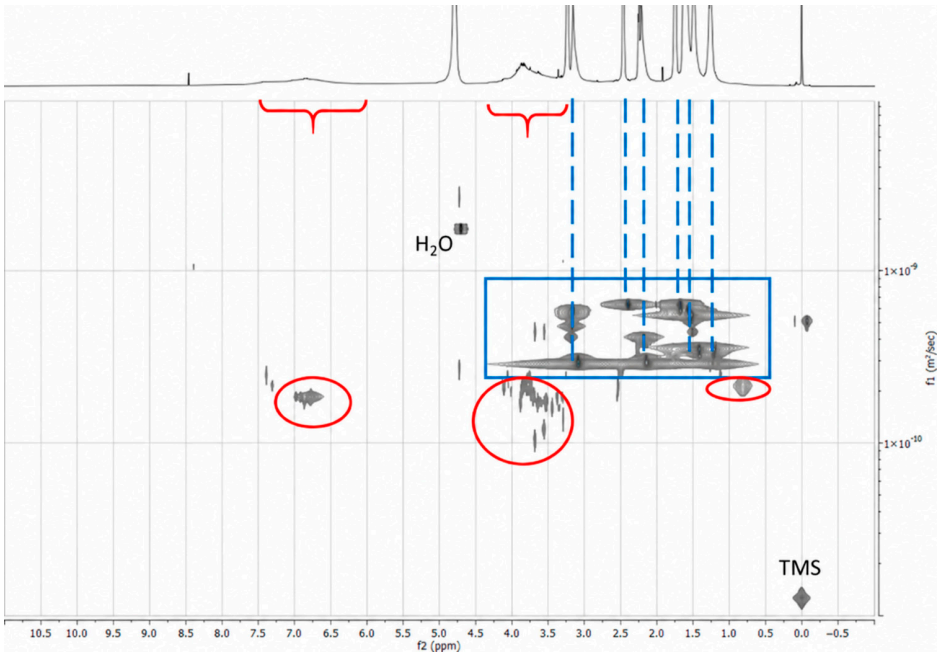


Figure 3. DOSY experiment on PA6-5L, PA6 oligomer signals (highlighted blue) and lignin signals (red).

Finally, Figure S23 reports the HSQC analysis of PA6-5L. The spectrum is dominated by the intensity of the sharp signals of PA6 oligomers, while lignin signals are barely detectable. Concerning lignin-related regions, both the aromatic and the oxidized aliphatic ones do not show any additional relevant signal, corroborating the absence of new covalent bonds between lignin and PA6.

The NMR tests confirm the qualitative structure of lignosulfonate as an architecture presenting extensive oxidized moieties able to potentially interact with polar groups present in PA6. While the NMR analysis of the microcomposites does not show substantial differences, a hot water-soluble fraction retrieved from the materials can be used to investigate possible PA6 grafting occurring during polymer synthesis. While ^{1}H- and ^{13}C- spectra of the retrieved fractions show the concurrent presence of lignin and PA6 oligomers, DOSY and HSQC analysis do not provide proof of any chemical linkage between extracted lignin and PA6 oligomers.

3.3. Differential Scanning Calorimetry (DSC)

DSC thermograms of the prepared composites and the corresponding results are respectively displayed in Figure 4a–c and Table 1.

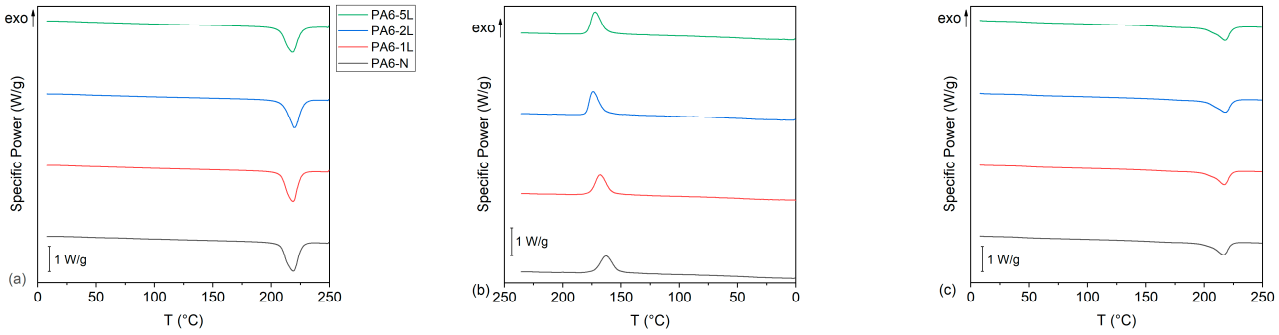


Figure 4. Differential scanning calorimetry (DSC) thermograms of neat PA6 and composite samples: (**a**) first heating scan; (**b**) cooling scan; (**c**) second heating scan.

Table 1. Results of the DSC tests of the prepared microcomposites, including melting temperature measured in the first heating scan ($T_{m,1}$), melting enthalpy measured in the first heating scan ($\Delta H_{m,1}$), crystallization temperature (T_c), and crystallinity of the PA6(χ).

Sample	$T_{m,1}$ (°C)	$\Delta H_{m,1}$ (J/g)	T_c (°C)	$T_{m,2}$ (°C)	χ (%)
PA6-N	218.9	86.4	162.8	216.5	45.5
PA6-1L	218.7	85.1	168.0	217.3	45.2
PA6-2L	219.9	79.2	174.0	218.1	42.6
PA6-5L	218.1	78.5	172.2	217.7	43.5

Some differences can be observed among samples. One endothermal peak that can be associated with PA6 melting is observed in all samples around 218 °C in both heating scans, with negligible variations among samples. One exothermal peak that is associated with PA6 crystallization is visible at approximately 170 °C, with a 10 °C increase between the neat sample and the 5 wt% sample. The expected inflection point corresponding to the T_g (which should be centered at approximately 60–70 °C [22,31]) is barely visible in all samples in heating scans, but it is so small that it cannot be identified with confidence. As expected, no peaks related to lignin are observed. These results are in accordance with previous studies on anionic PA6 and with the literature [13,31,41]. Calculated crystallinity ranges from 42.6 to 45.5%, with no relevant variations among samples, which is consistent with previous findings [22].

DSC evaluation indicates that the presence of lignin in the microcomposites does not significantly decrease PA6 crystallinity at higher filler concentrations; however, it may possibly anticipate the nucleation of aPA6 crystals from the melt. The slightly lower values of $T_{m,1}$ (approximately 218–219 °C) with respect to previous evaluation on aPA6 produced with the same setup [31,41] could indicate the presence of a different crystalline structure in the polyamide matrix, characterized by γ crystals ($T_m \approx 214$ °C) instead of α crystals ($T_m \approx 220$ °C), or a mixture of the two allotropic forms. However, the temperature difference is very small; this effect is likely attributed to the relatively high concentration of activator and initiator utilized for the matrix in this work.

Since no relevant variations are observed between neat and composite samples, it is possible to likely rule out the formation of a PA6–lignin copolymer in accordance with NMR evaluations, and the blend seems immiscible. However, the lignin concentrations utilized, which were limited by experimental constraints, would probably mask any trends, if present.

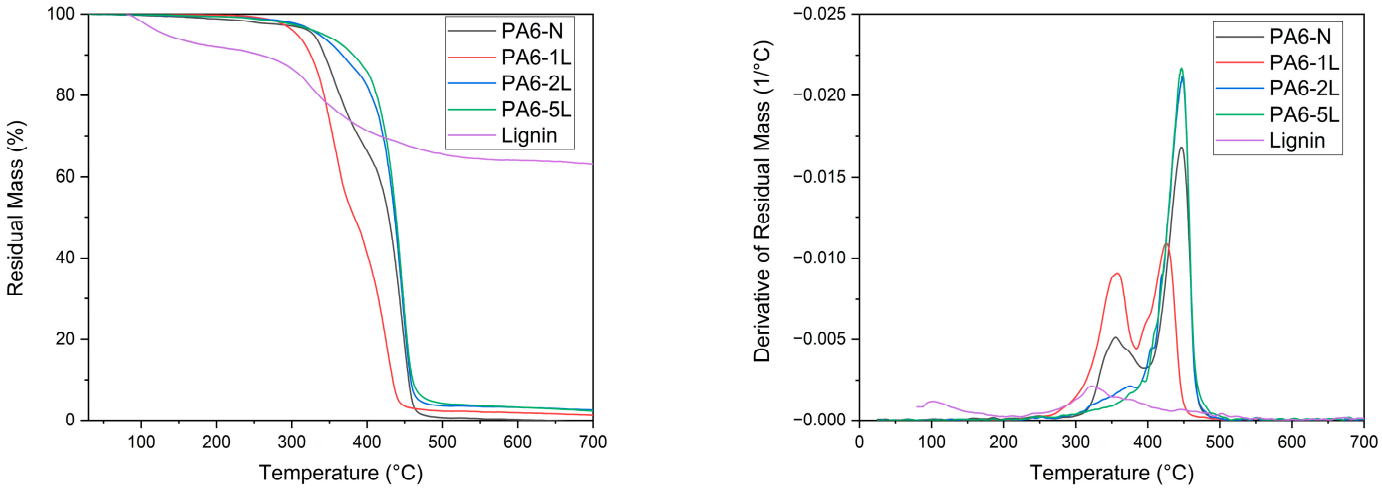
3.4. Thermogravimetric Analysis (TGA)

The main results of the TGA tests are reported in Figure 5a,b and Table 2.

The TGA curve of the as-received lignin shows two degradation events, one at approximately 100 °C and another one at 322 °C, and a continuous small decrease in mass, with a residual mass at 700 °C of 63.1%. The degradation peak centered around 100 °C is likely associated with residual humidity evaporation, while the peak at 322 °C is likely associated with the degradation of low- to medium-molecular-weight and volatile compounds or to the formation of volatiles from the breaking of side chains of lignin [42,43]. The TGA curves of the neat and microcomposite samples show two main degradation events at approximately 360 and 440 °C in accordance with previous evaluations on aPA6 composites [31]. The first degradation is much weaker in samples with a higher lignin fraction. The onset temperature of the degradation is increased for samples containing more than 2 wt% of lignin, indicating better thermal stability. Residual mass at 700 °C is higher in composites containing lignin with respect to the neat PA6 sample, but no clear trends can be observed. No significant variations can be detected in the temperatures of the degradation peaks in the DTG. A small

improvement in conversion degree is observed in composite samples with respect to the neat PA6.

The slight increase of conversion degree for these concentrations of lignin with respect to the neat matrix and the low porosity observed in SEM micrographs indicate improved processability of aPA6 composites with this specific matrix formulation (4.40/3.00 phr of C10/C20P) in the presence of this lignosulfonate filler. The flattening of the first PA6 peak is likely associated with a decrease in polydispersity and the transition from a mainly bimodal distribution of molecular weight to a unimodal distribution. For this reason, no values for T_{deg1} are reported in Table 2 for PA6-2L and PA6-5L. This could likely indicate an increase in average molecular weight of PA6 in the presence of lignin, although further analysis is needed to assess this point. Samples containing more than 2 wt% of lignin also show improved thermal stability with respect to neat and PA6-1L samples, as opposed to the results reported by Sallem-Idrissi et al. [30]. This could be related to the different nature of the matrix (aPA6 in this work and hydrolytic PA6 in [30]) and/or to the lower concentrations of lignin employed in the present work. The higher value for the residual mass at 700 °C detected for sample PA6-2L with respect to PA6-5L, this is probably linked to random fluctuations of concentration of thermal resistant components of the lignin within the composites.



(**a**) (**b**)

Figure 5. (**a**) TGA thermograms and (**b**) their derivative curves (DTG) for as-received lignin, neat PA6, and the relative microcomposites.

Table 2. Main results of the TGA measurements on as-received lignin, neat PA6, and the relative microcomposites, including conversion degree (*CD*), temperatures of the two main degradation peaks observed (T_{deg1} and T_{deg2}), the onset temperature of the degradation (T_{onset}), and the residual mass at 700 °C.

Sample	*CD* (%)	T_{deg1} (°C)	T_{deg2} (°C)	T_{onset} (°C)	Residual at 700 °C (%)
Lignin	–	322	–	–	63.1
PA6-N	98.0	355	447	330	0.0
PA6-1L	99.3	358	425	324	1.3
PA6-2L	99.0	–	448	392	2.6
PA6-5L	98.7	–	447	397	2.3

3.5. Quasi-Static Tensile Tests

Results of the quasi-static tensile tests are reported in Figures 6 and 7a–d.

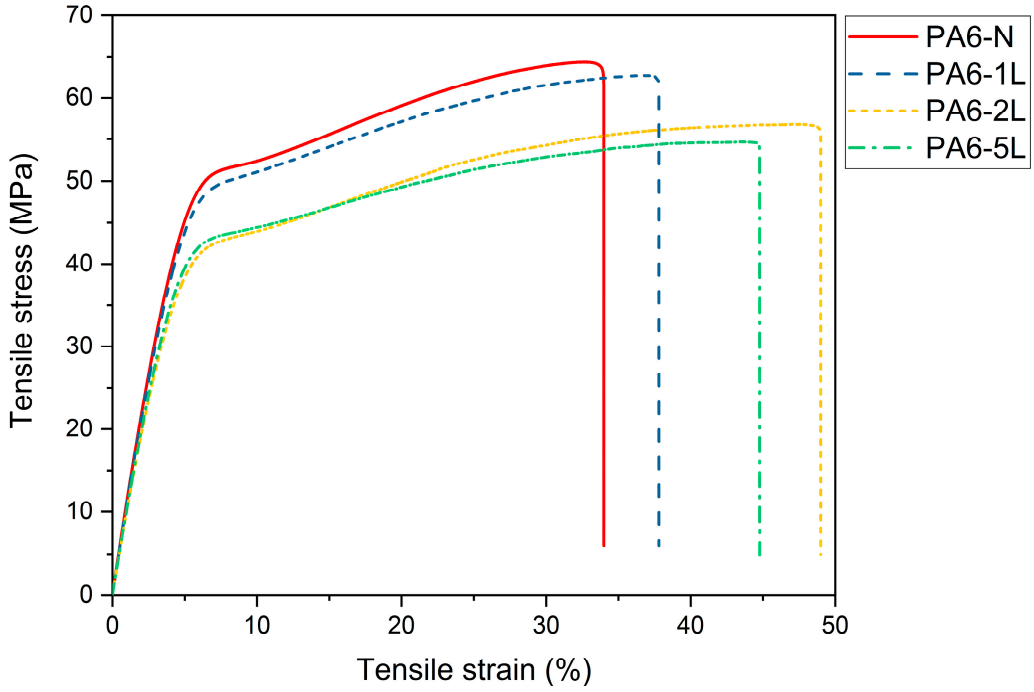


Figure 6. Representative stress–strain curves from quasi-static tensile tests on the neat PA6 and microcomposite samples.

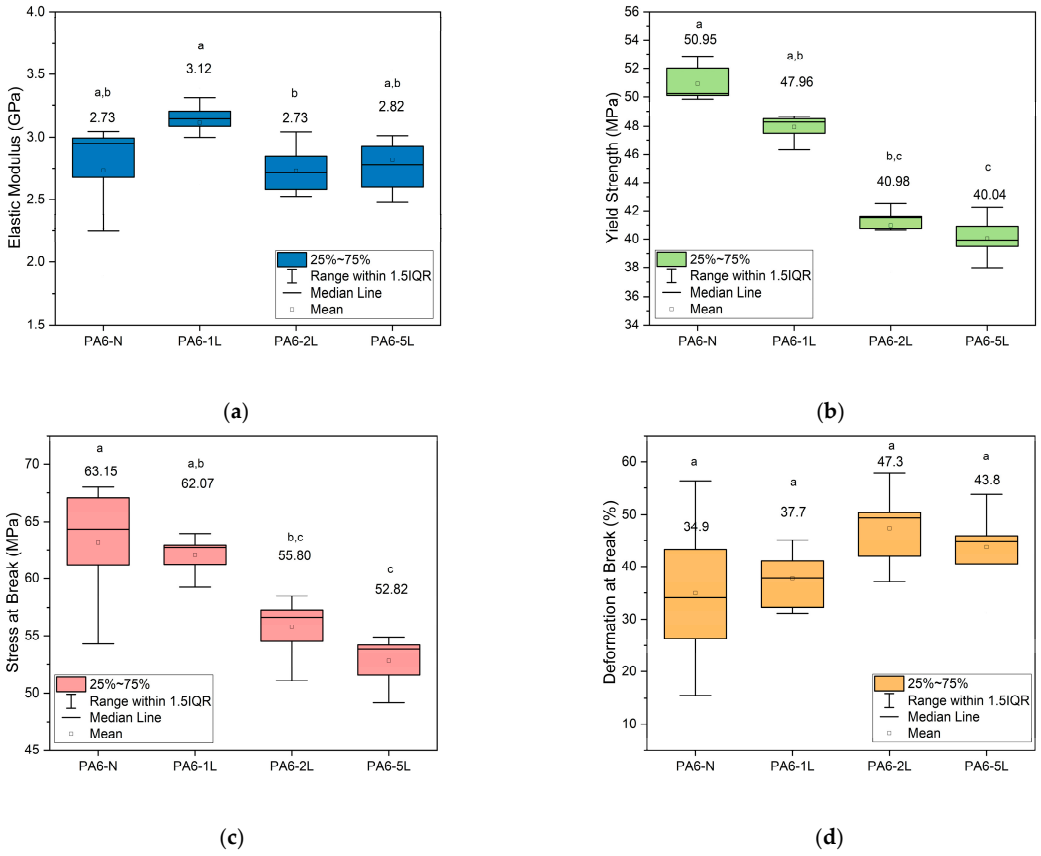


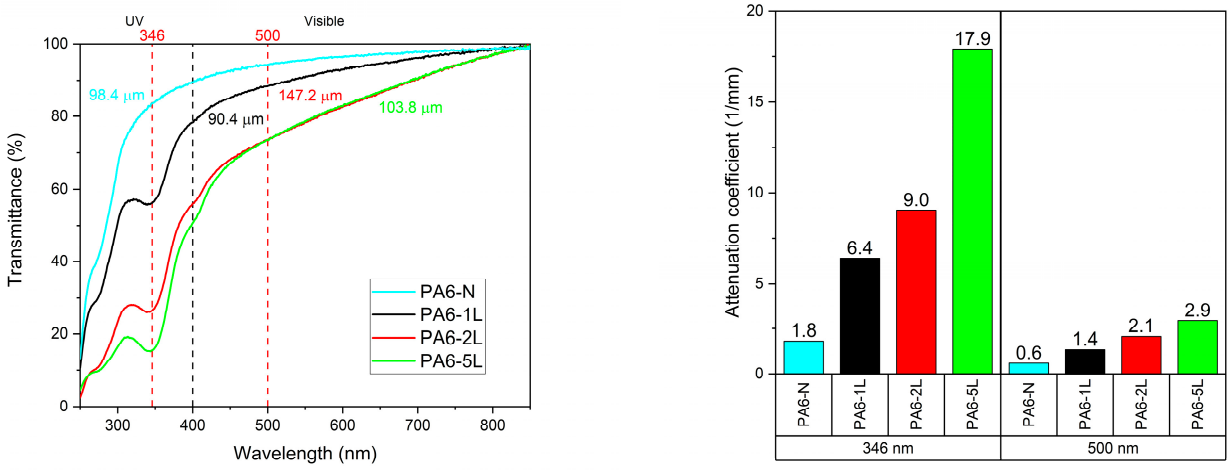
Figure 7. Boxplots of the quasi-static tensile properties of neat PA6 and microcomposite samples. The number reported over the boxplots represents the average value. Different letters above two boxplots indicate a statistically significant difference between them, according to post hoc Dunn's test. (**a**) Elastic modulus; (**b**) yield strength; (**c**) stress at break; (**d**) deformation at break.

Stress–strain curves shown in Figure 6 display the typical ductile behavior of aPA6 for all compositions. Results for the neat sample are comparable to those found in previous works on anionic PA6 [41]. From the boxplots in Figure 7a–d, it can be noticed that the elastic modulus and the deformation at break do not vary considerably among the samples, while a moderate decrease in yield strength (up to 21.4%) and stress at break (up to 16.3%) can be observed in the mean values at increasing lignin concentrations. Interestingly, the statistical dispersion of deformation at break values is reduced in microcomposite samples with respect to the neat PA6 matrix. Analysis by Kruskal–Wallis test confirms that there is statistically relevant difference among the tested samples for all the properties. Dunn's post hoc test highlights that there is statistically relevant difference between some couples of samples for elastic modulus, yield strength, and stress at break. Elastic modulus peaks at 1 wt% and then decreases up to 5 wt%, reaching values that are not statistically different to the neat matrix. For both yield strength and stress at break the values decrease with increasing filler content, with PA6-N and PA6-1L being statistically similar and PA6-2L and PA6-5L being statistically similar. Finally, deformation at break does not display statistically significant differences between the single pairs of samples according to Dunn's post hoc test, even though the Kruskal–Wallis test indicated statistically significant difference among the groups (p-value = 0.028). The results of the two tests for deformation at break are not contradictory, and they evidence overall difference among the groups, but they do not indicate significant differences between two specific pairs.

Overall, the tensile properties are not strongly negatively influenced by the addition of the biofiller, and the tough and ductile behavior of aPA6 is maintained, even at 5 wt% filler addition. The decreased dispersion of the values for elongation at break could be associated with improved predictability and reliability of the material, probably due to the preferential crack initiation that is observed within the lignin particles in SEM observations. The moderate decrease in stress at break in microcomposites with respect to neat PA6 is probably linked to the increase of intraparticle porosity and cracking apported by the brittle lignin filler.

3.6. UV–Visible Transmittance

The main results of the UV–visible spectrophotometry are reported in Figure 8a,b.



(**a**) (**b**)

Figure 8. Results of the UV–visible spectrophotometry on film samples. (**a**) Spectra of the neat PA6 and microcomposite samples, mean thicknesses of the film specimens are reported along with the curve; (**b**) attenuation coefficient values for selected wavelengths, 346 nm (UV spectrum), and 500 nm (visible spectrum), calculated according to Equation (3).

Lignin-filled samples show a marked decrease in transmittance in the UV range and a moderate decrease in the visible spectrum with respect to neat aPA6. Notably, the decrease in transmittance at 346 nm for microcomposites containing lignin with respect to neat PA6 samples is more marked. Higher concentrations of lignin produce films that are less transparent to UV radiation, but the difference between the PA6-2L and the PA6-5L is not as marked. This might indicate a threshold concentration of lignin (2 wt%) after which only a minor decrease in transmittance is obtained. Attenuation coefficient, calculated according to Equation (3), shows an increase of 894% at 346 nm (UV range) in sample PA6-5L with respect to the neat matrix at 346 nm but only of 383% at 500 nm (visible range).

The increased attenuation coefficient in the UV range for microcomposites is an important functional improvement, likely attributed to the UV-absorbing properties of lignin [20]. Decreased UV transparency, along with the well-known gas barrier capability of PA6 [44], could be employed in applications where it is used as encapsulation for UV-sensitive devices (such as sensors or outdoor electronics) or as technical packaging for UV-sensitive goods and chemicals. It is also worth noting that the relatively moderate increase in attenuation coefficient in the visible spectrum can be very beneficial for some applications.

UV shielding and UV stability are correlated, as discussed in [45]. However, further analysis would be necessary to properly assess the improvement of UV stability likely imparted to the aPA6 by the addition of lignin. UV stability is an under-utilized design parameter for polymers that can, however, have a strong influence on the long-term performance of the material and on its environmental impact [14]. Improved UV stability is possibly linked to extend life of the product and reduced microplastic formation due to the decrease of the kinetics of photooxidation of the polymer chain and therefore decreased embrittlement of the material during prolonged environmental exposure. This mechanism is considered one of the main causes for microplastic formation [14]. The prolonged life of the product is associated with lower maintenance and a lower carbon footprint, especially for outdoor applications.

4. Conclusions

The present study investigated the incorporation of sulfonated lignin powder at varying weight fractions (0, 1, 2, 5 wt%) in an anionic PA6 matrix for enhancing its functional properties. Composites were studied via several characterization methods, including SEM, NMR, DSC, TGA, tensile tests, and UV–visible spectroscopy.

The production process for the composites employed AROP of ε-caprolactam, a technique very sensitive to moisture and impurities. High yields of the polymerization reaction highlighted excellent processability and compatibility of the matrix and the biofiller. Such compatibility might be attributed to polar interactions and hydrogen bonds since NMR spectroscopy excluded the formation of chemical grafting of PA6 on the lignosulfonate particles. SEM analysis confirmed limited porosity but adequate dispersion of the filler in the matrix, confirming that the matrix-filler interaction is predominantly physical. A moderate decrease in yield strength (up to 21.4%) and stress at break (up to 16.3%), along with no relevant variations in thermal properties and crystallinity among neat and reinforced samples, indicated that the incorporation of lignin did not significantly alter the thermo-mechanical properties of PA6.

Notably, the addition of sulfonated lignin decreased markedly the optical transmission of the material, in particular in the UV range (with attenuation coefficient increased up to 894% at 346 nm), thus providing interesting tunable UV-shielding capabilities that could be employed, combined with the well-known gas barrier capabilities of PA6, in technical packaging or encapsulation of UV-sensitive devices and goods. Even though the present work did not investigate the resistance to UV radiation and weathering, the improved UV

attenuation, likely promoted by the absorption of the radiation by the lignosulfonates, might contribute to a decrease in photo-oxidation in the polymeric matrix and therefore possibly to a prolonged life cycle and decreased microplastic formation, strongly decreasing the environmental impact of the material. Moreover, the absence of chemical bonding between matrix and filler could allow for an easy separation of the two phases and therefore an improved recyclability via minor modifications to traditional recycling strategies. However, further melt reprocessing tests would be required to properly assess recyclability of the material.

Overall, this work demonstrated an easy route of production for high-performance, partially bio-based thermoplastic microcomposites that show promising functional properties without substantially compromising the mechanical and thermal resistance of the neat PA6. Future work should focus on further characterization of impact properties and of other functional properties, such as flammability, and possibly on improving matrix-filler compatibility to preserve the mechanical properties and improve multifunctionality of the material so as to optimize material usage in technical applications for improved environmental benefit.

Supplementary Materials: The following supporting information can be downloaded at https://www.mdpi.com/article/10.3390/jcs10110576/s1: Figure S1: HSQC spectrum of the starting lignin in D_2O; Figure S2: ^{1}HNMR spectrum of the starting lignin in D_2O; Figure S3: DOSY experiment for the starting lignin in D_2O; Figure S4: ^{1}HNMR spectrum of PA6-N in d_2-formic acid/$CDCl_3$ (9:1); Figure S5: ^{13}CNMR spectrum of PA6-N in d_2-formic acid/$CDCl_3$ (9:1); Figure S6: ^{1}HNMR spectrum of PA6-1L in d_2-formic acid/$CDCl_3$ (9:1); Figure S7: ^{13}CNMR spectrum of PA6-1L in d_2-formic acid/$CDCl_3$ (9:1); Figure S8: ^{1}HNMR spectrum of PA6-2L in d_2-formic acid/$CDCl_3$ (9:1); Figure S9: ^{13}CNMR spectrum of PA6-2L in d_2-formic acid/$CDCl_3$ (9:1); Figure S10: ^{1}HNMR spectrum of PA6-5L in d_2-formic acid/$CDCl_3$ (9:1); Figure S11: ^{13}CNMR spectrum of PA6-5L in d_2-formic acid/$CDCl_3$ (9:1); Figure S12: ^{1}HNMR spectrum of PA6-N in D_2O; Figure S13: ^{13}CNMR spectrum of PA6-N in D_2O; Figure S14: DOSY of PA6-N in D_2O; Figure S15: ^{1}HNMR spectrum of PA6-1L in D_2O; Figure S16: ^{13}CNMR spectrum of PA6-1L in D_2O; Figure S17: DOSY of PA6-1L in D_2O; Figure S18: ^{1}HNMR spectrum of PA6-2L in D_2O; Figure S19: ^{13}CNMR spectrum of PA6-2L in D_2O; Figure S20: DOSY of PA6-2L in D_2O; Figure S21: ^{1}HNMR spectrum of PA6-5L in D_2O; Figure S22: ^{13}CNMR spectrum of PA6-5L in d_6-DMSO; Figure S23: HSQC of PA6-5L in D_2O; Figure S24: DOSY of PA6-5L in D_2O.

Author Contributions: Conceptualization, G.F., C.G. and A.D.; methodology, G.F. and C.G.; software, R.M. and C.G.; validation, G.F. and C.G.; formal analysis, M.P.; investigation, M.P., R.M., A.S., E.Z. and P.S.; resources, G.F., A.D. and C.G.; data curation, G.F.; writing—original draft preparation, M.P.; writing—review and editing, R.M., C.G., G.F. and A.D.; visualization, M.P., R.M. and C.G.; supervision, G.F., C.G. and A.D.; project administration, G.F., C.G. and A.D.; funding acquisition, G.F., C.G. and A.D. All authors have read and agreed to the published version of the manuscript.

Funding: The work has been produced with the co-funding of the European Union, FSE-REACT-EU, PON Research and Innovation (Action IV.6—Green) 2014–2020 DM1062/2021.

Data Availability Statement: The raw data supporting the conclusions of this article will be made available by the authors on request.

Acknowledgments: The authors would like to acknowledge Claudia Gavazza and Alfredo Casagranda for their technical support. P.S. kindly acknowledges the FRUITOMICS FESR 2014–2020 program funded by the Autonomous Province of Trento.

Conflicts of Interest: The authors declare no conflicts of interest.

References

1. Calvin, K.; Dasgupta, D.; Krinner, G.; Mukherji, A.; Thorne, P.W.; Trisos, C.; Romero, J.; Aldunce, P.; Barrett, K.; Blanco, G.; et al. *IPCC, 2023: Climate Change 2023: Synthesis Report. Contribution of Working Groups I, II and III to the Sixth Assessment Report of the Intergovernmental Panel on Climate Change*; Core Writing Team, Lee, H., Romero, J., Eds.; IPCC: Geneva, Switzerland, 2023; pp. 35–115.
2. Crutzen, P.; Stoermer, E. The anthropocene. In *The Future of Nature*; Yale University Press: New Haven, CT, USA, 2000; Volume 41, pp. 17–18.
3. Ajayi, N.E.; Rusnakova, S.; Ajayi, A.E.; Ogunleye, R.O.; Agu, S.O.; Amenaghawon, A.N. A comprehensive review of natural fiber reinforced Polymer composites as emerging materials for sustainable applications. *Appl. Mater. Today* **2025**, *43*, 102666. [CrossRef]
4. van Rijswijk, K.; Bersee, H.E.N. Reactive processing of textile fiber-reinforced thermoplastic composites–An overview. *Compos. Part A Appl. Sci. Manuf.* **2007**, *38*, 666–681. [CrossRef]
5. Ageyeva, T.; Sibikin, I.; Kovács, J.G. A Review of Thermoplastic Resin Transfer Molding: Process Modeling and Simulation. *Polymers* **2019**, *11*, 1555. [CrossRef] [PubMed]
6. Kanu, N.J.; Gupta, E.; Vates, U.K.; Singh, G.K. Self-healing composites: A state-of-the-art review. *Compos. Part A Appl. Sci. Manuf.* **2019**, *121*, 474–486. [CrossRef]
7. Di Liberto, D.; Tauro, A.; Perin, D.; Savioli, I.; Coser, M.; Fredi, G.; Rigotti, D.; Dorigato, A.; Pegoretti, A. Impact-modified polyamide 11/carbon nanotubes 3D printing and potential enhancement of toughness in fiber reinforced polymers. *J. Reinf. Plast. Compos.* **2026**, *45*, 2036–2050. [CrossRef]
8. Perin, D.; Odorizzi, G.; Dorigato, A.; Pegoretti, A. Development of Polyamide 6 (PA6)/Polycaprolactone (PCL) Thermoplastic Self-Healing Polymer Blends for Multifunctional Structural Composites. *Appl. Sci.* **2022**, *12*, 12357. [CrossRef]
9. Perin, D.; Botta, L.; Rigotti, D.; Dorigato, A.; Fredi, G.; Pegoretti, A. Tuning the Compatibilizer Content and Healing Temperature in Thermally Mendable Polyamide 6/Cyclic Olefin Copolymer Blends. *Polymers* **2025**, *17*, 280. [CrossRef] [PubMed]
10. Perin, D.; Fredi, G.; Russo, P.; Pegoretti, A.; Dorigato, A. Intrinsic self-healing of polyamide 6/carbon fiber thermoplastic laminates. *Compos. Part A Appl. Sci. Manuf.* **2026**, *201*, 109393. [CrossRef]
11. Kashani Rahimi, S.; Otaigbe, J.U. Natural cellulose fiber-reinforced polyamide 6 thermoplastic composites prepared via in situ anionic ring-opening polymerization. *Polym. Compos.* **2019**, *40*, 1104–1116. [CrossRef]
12. Ageyeva, T.; Sibikin, I.; Karger-Kocsis, J. Polymers and Related Composites via Anionic Ring-Opening Polymerization of Lactams: Recent Developments and Future Trends. *Polymers* **2018**, *10*, 357. [CrossRef] [PubMed]
13. van Rijswijk, K.; Bersee, H.E.N.; Beukers, A.; Picken, S.J.; van Geenen, A.A. Optimisation of anionic polyamide-6 for vacuum infusion of thermoplastic composites: Influence of polymerisation temperature on matrix properties. *Polym. Test.* **2006**, *25*, 392–404. [CrossRef]
14. Chamas, A.; Moon, H.; Zheng, J.; Qiu, Y.; Tabassum, T.; Jang, J.H.; Abu-Omar, M.; Scott, S.L.; Suh, S. Degradation Rates of Plastics in the Environment. *ACS Sustain. Chem. Eng.* **2020**, *8*, 3494–3511. [CrossRef]
15. Papparotto, M.; Gavazza, C.; Matteotti, P.; Fambri, L. Seasonal Comparative Monitoring of Plastic and Microplastic Pollution in Lake Garda (Italy) Using Seabin During Summer–Autumn 2024. *Microplastics* **2025**, *4*, 44. [CrossRef]
16. Du, S.; Wei, Y.; Ahmed, S.; Zhou, F.; Tan, Y.; Li, Y.; Wang, M.; Chen, X.; Zhou, W. Enhanced thermal stability and UV resistance of polyamide 6 filament fabric via in-situ grafting with methyl methacrylate. *Colloids Surf. A Physicochem. Eng. Asp.* **2022**, *651*, 129371. [CrossRef]
17. Zhou, C.; Guo, R.; Wang, Y.; Wang, H.; Shao, X.; Li, N. Effective preparation of SiO_2-TiO_2@PA6 fabric with enhanced ultraviolet resistance and thermal insulation performances. *Colloids Surf. A Physicochem. Eng. Asp.* **2025**, *727*, 138261. [CrossRef]
18. Liu, J.; Qiu, S.; Qi, P.; Sun, J.; Li, H.; Gu, X.; Zhang, S. Constructing a Fully Biobased Coating to Improve the Flame Retardancy, Antibacterial Properties, and UV Resistance of Polyamide 6 Fabrics. *ACS Appl. Eng. Mater.* **2023**, *1*, 268–277. [CrossRef]
19. Dai, S.; Yan, F.; Guo, J.; Li, M.; Zhao, Y.; Liu, Y.; Liu, L.; Ao, Y. A novel bio-based hyperbranched waterborne polyurethane sizing agent with superior UV-resistance and interfacial properties for CF/PA6 composites. *Compos. Sci. Technol.* **2023**, *242*, 110214. [CrossRef]
20. Dias, O.A.T.; Negrão, D.R.; Gonçalves, D.F.C.; Cesarino, I.; Leão, A.L. Recent approaches and future trends for lignin-based materials. *Mol. Cryst. Liq. Cryst.* **2017**, *655*, 204–223. [CrossRef]
21. Rahman, M.Z.; Wang, X.; Cai, W.; Song, L.; Fei, B.; Hu, Y. Sustainable lignosulfonate-modified PA6.6 fabrics to improve durable flame retardancy, hydrophilicity and mechanical performance. *Int. J. Biol. Macromol.* **2024**, *280*, 135952. [CrossRef] [PubMed]
22. Sorze, A.; Miani, R.; Gioia, C.; Fredi, G.; Dorigato, A. Improved Thermo-Mechanical and Flame Resistance Behaviour of Polyamide 6/Lignin Microcomposites. *Macromol* **2026**, *6*, 18. [CrossRef]
23. Bittencourt, P.; Fernandes, D.; Silva, M.; Lima, M.; Hechenleitner, A.; Gómez Pineda, E.A. Lignin Modified by Formic Acid on the PA6 Films: Evaluation on the Morphology and Degradation by UV Radiation. *Waste Biomass Valorization* **2010**, *1*, 323–328. [CrossRef]

24. Hu, L.; Stevanovic, T.; Rodrigue, D. Compatibilization of kraft lignin-polyethylene composites using unreactive compatibilizers. *J. Appl. Polym. Sci.* **2014**, *131*, 41040. [CrossRef]
25. Dias, O.A.T.; Negrão, D.R.; Silva, R.C.; Funari, C.S.; Cesarino, I.; Leao, A.L. Studies of lignin as reinforcement for plastics composites. *Mol. Cryst. Liq. Cryst.* **2016**, *628*, 72–78. [CrossRef]
26. Hilburg, S.L.; Elder, A.N.; Chung, H.; Ferebee, R.L.; Bockstaller, M.R.; Washburn, N.R. A universal route towards thermoplastic lignin composites with improved mechanical properties. *Polymer* **2014**, *55*, 995–1003. [CrossRef]
27. Spiridon, I.; Leluk, K.; Resmerita, A.M.; Darie, R.N. Evaluation of PLA–lignin bioplastics properties before and after accelerated weathering. *Compos. Part B Eng.* **2015**, *69*, 342–349. [CrossRef]
28. Luo, S.; Cao, J.; McDonald, A.G. Interfacial Improvements in a Green Biopolymer Alloy of Poly(3-hydroxybutyrate-co-3-hydroxyvalerate) and Lignin via in Situ Reactive Extrusion. *ACS Sustain. Chem. Eng.* **2016**, *4*, 3465–3476. [CrossRef]
29. Chung, Y.-L.; Olsson, J.V.; Li, R.J.; Frank, C.W.; Waymouth, R.M.; Billington, S.L.; Sattely, E.S. A Renewable Lignin–Lactide Copolymer and Application in Biobased Composites. *ACS Sustain. Chem. Eng.* **2013**, *1*, 1231–1238. [CrossRef]
30. Sallem-Idrissi, N.; Sclavons, M.; Debecker, D.P.; Devaux, J. Miscible raw lignin/nylon 6 blends: Thermal and mechanical performances. *J. Appl. Polym. Sci.* **2016**, *133*, 42963. [CrossRef]
31. Valentini, M.; De Almeida, O.; Kakkonen, M.; Kalinka, G.; Dorigato, A.; Kallio, P.; Fredi, G. Effect of fiber surface state on the thermomechanical and interfacial properties of in situ polymerized polyamide 6/basalt fiber composites. *Compos. Part A Appl. Sci. Manuf.* **2025**, *190*, 108681. [CrossRef]
32. *UNI EN ISO 527-1:2019*; Materie Plastiche—Determinazione Delle Caratteristiche a Trazione—Parte 1: Principi Generali. UNI—Ente Italiano di Normazione: Milano, Italy, 2019.
33. *UNI EN ISO 527-2:2012*; Materie Plastiche—Determinazione Delle Caratteristiche a Trazione—Parte 2: Condizioni di Prova per Materie Plastiche per Stampaggio ed Estrusione. UNI—Ente Italiano di Normazione: Milano, Italy, 2012.
34. Asikanius, B.; Liitiä, T.; Rigo, D.; Giummarella, N.; Slättegård, R.; Österberg, M. Adsorption of sulphonated lignin-carbohydrate complexes (LCCs) onto cellulose surfaces. *Carbohydr. Polym. Technol. Appl.* **2024**, *8*, 100591. [CrossRef]
35. Wang, S.; Ren, X.; Dai, J.; Gan, T.; Qi, J.; Chen, L.; Xie, J.; Pan, H. Comprehensive analysis of the molecular structure of lignin from microwave-assisted fractionation. *Ind. Crops Prod.* **2026**, *239*, 122529. [CrossRef]
36. Lv, X.; Li, Q.; Jiang, Z.; Wang, Y.; Li, J.; Hu, C. Structure characterization and pyrolysis behavior of organosolv lignin isolated from corncob residue. *J. Anal. Appl. Pyrolysis* **2018**, *136*, 115–124. [CrossRef]
37. Watumlawar, E.; Park, B.-D. Activation of methoxy group of hardwood kraft lignin via cross-coupling and crosslinking for lignin-based wood adhesives. *Int. J. Biol. Macromol.* **2025**, *315*, 144670. [CrossRef] [PubMed]
38. Tricker, A.W.; Stellato, M.J.; Kwok, T.T.; Kruyer, N.S.; Wang, Z.; Nair, S.; Thomas, V.M.; Realff, M.J.; Bommarius, A.S.; Sievers, C. Similarities in Recalcitrant Structures of Industrial Non-Kraft and Kraft Lignin. *ChemSusChem* **2020**, *13*, 4624–4632. [CrossRef] [PubMed]
39. Lu, Q.; Yang, C.; Song, X. Preparation of S, N codoped lignin composite iron phthalocyanine as an efficient oxygen reduction reaction catalyst by one-pot method and application to high-performance lignin fuel cells. *J. Colloid Interface Sci.* **2026**, *701*, 138782. [CrossRef] [PubMed]
40. Gioia, C.; Lo Re, G.; Lawoko, M.; Berglund, L. Tunable Thermosetting Epoxies Based on Fractionated and Well-Characterized Lignins. *J. Am. Chem. Soc.* **2018**, *140*, 4054–4061. [CrossRef] [PubMed]
41. Fredi, G.; Broggio, L.; Valentini, M.; Bortolotti, M.; Rigotti, D.; Dorigato, A.; Pegoretti, A. Decoding the interplay of mold temperature and catalysts concentration on the crystallinity and mechanical properties of anionic polyamide 6: A combined experimental and statistical approach. *Polymer* **2024**, *311*, 127562. [CrossRef]
42. Muir, V.; Tripathi, N.; Rodriguez-Uribe, A.; Mohanty, A.K.; Misra, M. Sustainable biocomposites from pyrolyzed lignin and recycled nylon 6 with enhanced flame retardant behavior: Studies on manufacturing and quality performance evaluation. *SPE Polym.* **2024**, *5*, 277–292. [CrossRef]
43. Mishra, R.K.; Lu, Q.; Mohanty, K. Thermal behaviour, kinetics and fast pyrolysis of Cynodon dactylon grass using Py-GC/MS and Py-FTIR analyser. *J. Anal. Appl. Pyrolysis* **2020**, *150*, 104887. [CrossRef]
44. Wang, W.; Zhao, G.; Ma, X.; Ren, D.; Nie, M.; Han, R. Polyamide 6 as a Liner Material for Type IV Hydrogen Storage Cylinders: Performance Challenges and Modification Strategies. *Polymers* **2025**, *17*, 1848. [CrossRef] [PubMed]
45. Zhang, Y.; Naebe, M. Lignin: A Review on Structure, Properties, and Applications as a Light-Colored UV Absorber. *ACS Sustain. Chem. Eng.* **2021**, *9*, 1427–1442. [CrossRef]

Disclaimer/Publisher's Note: The statements, opinions and data contained in all publications are solely those of the individual author(s) and contributor(s) and not of MDPI and/or the editor(s). MDPI and/or the editor(s) disclaim responsibility for any injury to people or property resulting from any ideas, methods, instructions or products referred to in the content.